Tailoring slow light properties by shifting the innermost rows of holes in photonic crystal waveguides with ring-shaped holes

F. BAGCI, B. AKAOGLU*
Department of Engineering Physics, Faculty of Engineering, Ankara University, 06100 Besevler, Ankara, Turkey

A silicon ring-shaped photonic crystal waveguide embedded in silica is proposed and the effects of shifting the first and the second innermost rows towards the line-defect on slow light properties are systematically investigated by plane-wave expansion method. The first and second rows affect the slow light characteristics differently, which offers a strategy to design flatter bands. The behavior of slow light generation in ring-shaped photonic crystal waveguides against row shifting is clarified and a structural strategy for obtaining higher group index and less group velocity dispersion is put forward. Slow wave propagation is also verified by finite-difference time-domain calculations.

(Received May 21, 2013; accepted May 15, 2014)

Keywords: Photonic crystal waveguide, Slow light, Group index, Plane-wave expansion method, Finite-difference time-domain method

1. Introduction

There is a growing interest on slow light technology for its great variety of applications in optical buffering, optical signal processing and optical storing which lead the way into future's all-optical communication and information processing systems [1-3]. Photonic crystal waveguides (PCWs) are regarded as promising systems for slow light due to their compatibility on-chip integration, room temperature operation, tailorable wide bandwidth and dispersion-free propagation [2,3]. However, slow light, naturally occurring near the band edges of these structures, is restricted to a narrow bandwidth region and shows great group velocity dispersion (GVD) which causes the degradation of optical signals [4,5]. A variety of design approaches have been proposed to eliminate these drawbacks, such as changing the width of the W1 PCW [4,6,7], changing the radius of holes [3,8-11], using ring-shaped holes for the whole lattice [12] or only at the first [13,14] or first two rows [15] and changing the position of the first or first two rows in lateral [16,17], in perpendicular [18,19] or both directions [20] to the line-defect or solely shifting the third innermost rows of air holes [21].

In one of these studies [18], the first two innermost rows of holes of an air-bridged W1 PCW are shifted towards the line-defect systematically and almost constant group index-bandwidth products have been obtained for a broad range of different group indices. In our study, we looked for a similar behavior for a PCW with first innermost rows of ring-shaped holes in a silica-clad geometry. It should be noted that shifting the rows is usually preferred to changing the radius of holes in terms of fabrication control [18]. In addition, ring-shaped holes are attractive due to their enhanced refractive index sensing property [12]. Silica-clad PCWs are CMOS-compatible and technologically preferable to air-bridged PCWs for application point of views, such as Mach-Zehnder optical modulator [22] and optical switch [23] designs. The size of the MZM phase-shift modulators can be shortened to sizes comparable to micro-ring and electro-absorption modulators by employing slow light with shifted rows [22]. Lattice shifted PCWs in silica claddings were demonstrated for the first time for nonlinear enhancement purposes in [24]. In this study, by changing the position of the first and second rows adjacent to the line-defect separately and in combination, the mechanism of controlling slow light properties has been investigated. We point that shiftings of the first and second rows have different impacts on group index-frequency curves and are rather associated with different sections of the guided mode that offer a strategy to design flatter bands.

2. Waveguide design and modeling

A silicon photonic crystal slab structure with silica upper and bottom claddings is proposed as the basic structure. Silica-clad PCWs have mechanical stability, are insensitive to environmental contamination and can be easily integrated with electronic components on a single chip [25]. The holes of the first rows adjacent to the line-defect are chosen as ring-shaped holes with 0.34a outer and 0.19a inner radii to possess a constant slow light frequency region and the background holes are arranged as holes with the same radius as the outer radius of the rings, as shown in Fig. 1. Since the PC slab structure is embedded in the silica, the holes are filled with the silica that has a refractive index of 1.45. The shifts of first rows

are denoted as s1 and the shifts of second rows are denoted as s2 (Fig. 1). The shifts of rows towards the waveguide center are remarked with a positive sign and those away from the waveguide center are remarked with a negative sign. s1 is changed from 0.02a to -0.08a and s2 is changed from -0.02a to 0.08a. According to our observations on slow light with ring-shaped PCWs, in this study s1 shifts are dealt in a different shifting interval than [18] and the change of slow light properties under narrower line-width PCWs (W0.8) is also taken into account. First rows are not approached to the line-defect more than 0.02a because narrower line-widths increase the overlap of the mode field with the holes, which in turn, increase the scattering loss [26]. A general rule for obtaining the desired group index-frequency curves in these structures has also been put forward by examining various combinations of shifts in detail.

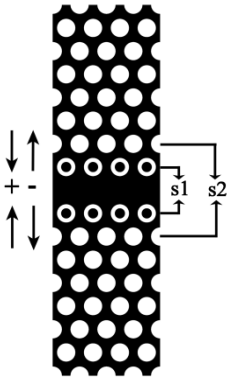

Fig. 1. Schematic picture of the photonic crystal waveguide structure. First row shifts are denoted as s1 and second row shifts are denoted as s2. Rows are shifted perpendicular to the line-defect.

Only vertically-even TE-like modes are considered since efficient coupling into the structure can only be realized for these modes [6]. The dispersion graphs for TE-like guided bands are calculated by two dimensional plane-wave expansion (PWE) method, employing MIT photonic bands package (MPB) [27] with a slab equivalent effective index of 2.98 [28]. The supercell size in the PWE calculations is set to a×17a, which is sufficiently large to neglect the coupling between adjacent software generated waveguides. The group index and group velocity dispersion values are obtained by using a built-in function of MPB. The pulse shape in the time domain is also analyzed and the group index obtained in the PWE method is confirmed by finite-difference time-domain (FDTD) calculations [29].

2.1. Figure of merits

There are some parameters indicating the performance of slow light in photonic crystal structures. The most important issue in slow light performance is the group velocity or group index whose magnitude indicates how slow light is. The group velocity is defined as,

$$\vartheta_G = \frac{d\omega}{dk} \tag{1}$$

The magnitude of the group velocity at a specific wave-vector can be obtained from the slope of the dispersion curve at that point.

The group index is inversely proportional to the group velocity and is defined by,

$$n_G = \frac{c}{\vartheta_G} \tag{2}$$

Since group index and bandwidth are inversely related, normalized delay-bandwidth product (NDBP), the product of average group index and normalized bandwidth, is introduced as a figure-of-merit,

$$NDBP = < n_G > \times \Delta\omega / \omega \tag{3}$$

where $\Delta\omega$ is the frequency bandwidth, ω denotes the central normalized frequency and $<n_G>$ is the averaged group index defined by,

$$< n_G >= \int_{\omega_0}^{\omega_0+\Delta\omega} n_G(\omega) d\omega / \Delta\omega \tag{4}$$

In the calculation of average group index, the limits of bandwidth are determined within the ±10% range of the minimum group index in this study.

Second order dispersion, defined as $d(dk/d\omega)^{-1}/d\omega$ is also evaluated as a figure-of-merit indicating the slow light performance. High group velocity dispersion severely distorts the waveform of low speed optical signals and makes slow light useless whatever the group velocity and bandwidth of light is [5].

3. Results and discussions

3.1. Dispersion and group index characteristics

There exist two different modes in the guided bands of photonic crystal waveguides [6]. These modes can be distinguished by their mode profiles. The index guided mode, which occurs at smaller wave numbers, has most of its energy concentrated in the waveguide, whereas the energy of gap guided mode extends deeper into the photonic crystal [6,7]. The anticrossing (intersection point) between these modes is very sensitive to the variation of properties of holes/rods adjacent to the waveguide, especially the two innermost rows [8].

First, only the effect of shifting of first rows adjacent to the line-defect is considered. The dispersion and group index characteristics for s2=0 is shown in Fig. 2(a) and (b), respectively. As the first rows move away from the line-defect, the width of line-defect increases which leads to decrease in the frequencies of guided modes. The shape of the n_G-frequency curves can be qualitatively determined

from the shape of the dispersion curve of the guided mode. There is an abrupt decrease of frequency as the wave-vector increases for the index-guided mode region. Since the $\Delta k/\Delta\omega$ is small, the n_G values are small in the high frequency region. When the first rows are moved away from the line-defect, the curvature of the guided band in the gap-guided region around $k=0.37(a/2\pi)$ changes its shape from down facing to linear and then to up-facing, due to interaction with the dielectric continuum. This upward-facing, which starts at s1=-0.02a, becomes more prominent as the s1 shifts increase in negative direction. As the curvature of the guided band becomes up-facing, the frequency increases weakly in the unit wave-vector change. This fact changes the step-like character of the n_G-frequency curve to U-shape for large absolute shifts of s1. The average group index decreases from 25.26 to 17.68, while the bandwidth increases from 11.37 nm to 32.13 nm.

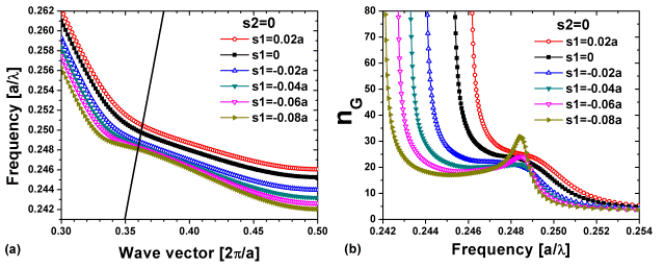

Fig. 2(a) Dispersion and (b) group index characteristics of the PCW with one row of ring-shaped holes adjacent to the line-defect for various shifts of first innermost rows when s2=0.

Second, the effect of shifting of second rows adjacent to the line-defect is taken into account for s1=0. The dispersion and group index characteristics for s1=0 is shown in Fig. 3(a) and (b), respectively. As the second rows approach to the line-defect, the frequency of the guided modes at the gap-guided part increases. Since there is no variation in the first rows adjacent to the line-defect, the character of index-guided mode remains almost the same. This fact causes the slope of dispersion curves to decrease, leading a substantial increase in the group index values. The average group indices increase from 21.16 to 66.74 while the bandwidths decrease from 16.60 nm to 5.36 nm.

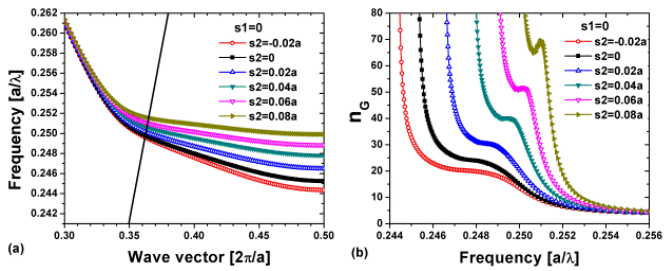

Fig. 3(a) Dispersion and (b) group index characteristics of the PCW with one row of ring-shaped holes adjacent to the line - defect for various shifts of second innermost rows when s1=0.

Finally, all combinations of shifts of s1 and s2 are considered. From the analysis of all shifts of s1 and s2, we deduce that shifting the first, second or both rows towards the line-defect leads to an increase in the group index. However, by shifting only the first rows, the group index can be increased in a more limited range. It is necessary to shift also the second rows towards the line-defect to reach greater group indices. This result is in agreement with the study of the systematic shift of two innermost rows of holes towards the line-defect in [18]. In a recent study, a group index between 15 and 30 and a normalized bandwidth between 0.6% and 1.2% ($\Delta\lambda$=9-18 nm) are obtained for 1.55 μm wavelength by shifting the third rows in lateral direction to the line-defect for the PCW structure in silica-clad [23]. By using two free parameters as s1 and s2, which denote the shifts in perpendicular direction to the line-defect, we obtain a larger group index range between 15.51 and 74.42 and a normalized bandwidth between 0.4% and 2.15% ($\Delta\lambda$=6.21 nm-25.36 nm) for this wavelength.

It is observed that first rows and second rows affect the group index characteristics differently. To compare the effect of s1 and s2 shifts on n_G-frequency curves of (s1;s2), one (s1;s2) combination can be chosen as a reference and shifts can be changed in equal amounts for s1 and s2. An example is given in Fig. 4 for (s1;s2)=(0.02a; 0.06a). As the first rows of rings approach to the line-defect, the n_G values and frequency of guided mode increase with a change in the n_G-frequency curve from U-shape to shoulder-like shape (Fig. 4(a)). However, as the second rows of holes move towards the line-defect, the n_G and frequency of the guided mode increase, but the shape of the n_G-frequency curve keeps its form (Fig. 4(b)). Through the analysis, it is noticed that s2 shifts, when s1 is fixed, do not generally change the shape of n_G-frequency curves but increase or decrease the n_G value and frequency. This fact is more prominent for smaller absolute s1 values. Although first rows consist of ring-shaped holes with smaller air filling ratio inside, the shape of n_G curves is mainly determined by the shifts of first rows adjacent to the line-defect.

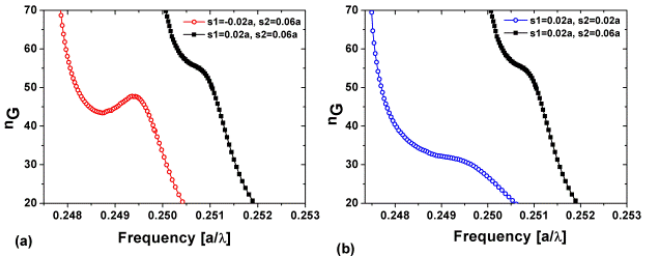

Fig. 4(a) Effects of first rows shift and (b) second rows shift on the group index characteristics of the PCW with one row of ring-shaped holes adjacent to the line-defect.

Another outcome of this analysis is that moving the innermost rows towards/from the line-defect results contrary behaviors on slow light properties. We examined this effect by applying equal amounts but opposite signs

for the first and second row shifts in Fig. 5. Decreasing s1 accompanied with an increase in s2 leads to different behaviors in the index-guided and gap-guided parts of the dispersion bands. The frequencies of index-guided modes decrease while the frequencies of gap-guided modes increase. Due to the shift of the anticrossing point to smaller wave numbers, the increase in frequency at the gap-guided mode starts to occur at smaller wave numbers as the absolute value of the shifts increases. Hence, the curvature of guided bands at the gap-guided region faces upward for the absolute values of s1 and s2 shifts greater than 0.02a. This behavior changes the shape of group index-frequency curve from step-like to U-shape and decreases the increase in group index. The amount of upward facing of dispersion curves at the gap-guided region can be decreased by choosing the absolute s1 value smaller than the s2 value. Hence, the n_G-frequency curve can be prevented from transforming into U-shape.

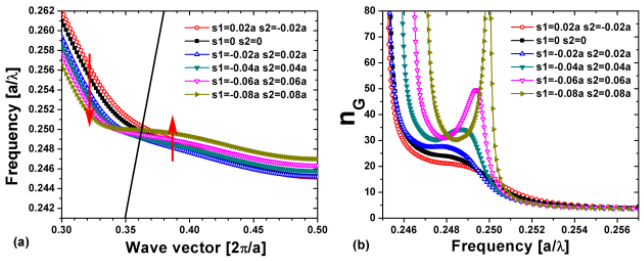

Fig. 5(a) Dispersion and (b) group index characteristics of the PCW with one row of ring-shaped holes adjacent to the line-defect for various shifts of first and second innermost rows. The shifting amounts are identical for the first and second row shifts, however their signs are opposite.

The behaviour of the dispersion curves against s1 and s2 shifts through opposite directions can be reasonably explained by considering the effective refractive index variation. As s1 increases in negative direction, the effective refractive index increases which leads to a decrease in the frequency of the index-guided mode. As s2 increases in positive direction, the effective refractive index decreases which leads to an increase in the frequency of the gap-guided mode. This situation shows that the first rows adjacent to the line-defect rather impact on index-guided parts while second rows adjacent to the line-defect rather impact on gap-guided parts of guided bands. The less impact of first rows on gap-guided region for larger negative shifts is reasonable since the first rows consist of ring-shaped holes with smaller air filling ratio. These outcomes can be utilized to design the desired shape of n_G-frequency curves and in turn, to minimize the higher-order dispersions.

The NDBPs are mapped as a function of s1 and s2 for the investigated PCW configurations in Fig. 6 and the average group index values are given on the plot as contours. In the color map, the red color represents the highest and the dark blue color represents the lowest NDBP value. In the columns of s2=0.08a, s1=-0.08a and s1=0.02a, the NDBP values are found to be low (0.15<NDBP<0.22). The reasons for low NDBP values reside mainly on two factors: The shape of n_G-frequency curves and low n_G values. When the n_G-frequency curves are U-shaped, the bandwidth measure of +10% and -10% of minimum group index turns out to be both +10% on the two sides of the U-curve, which means a decrease in the measure of bandwidth. It is noteworthy to point out that step-shaped n_G-frequency curves are preferred to U-shaped ones in terms of GVD and NDBP concerns. The abrupt change of NDBP from (-0.04a;0) to (-0.06a;-0.02a) stems from the change of the shape of n_G-frequency curve from step-like to U-shape, which makes the ±10% bandwidth criteria to turn into +10%. This point has not been emphasized in previous slow light studies in PCWs, though it limits the NDBP. As the amount of s1 shifts increases in negative direction, n_G-frequency curves are found to be turning into a more deep U-shapes. The maximum NDBP is found to be 0.4427 for s1=-0.04a due to large ratio of normalized bandwidth, since normalized bandwidth affects the value of NDBP more than the average group index.

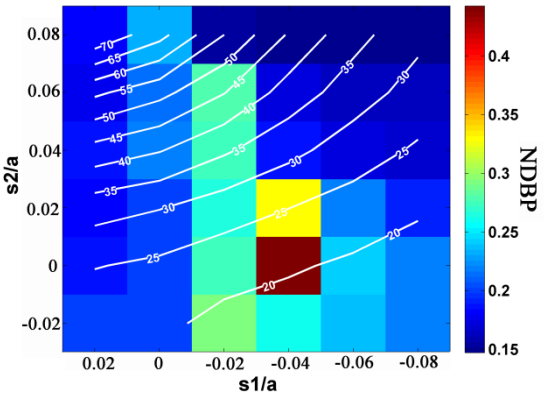

Fig. 6. Systematic scan of normalized delay-bandwidth products as a function of first and second innermost row shifts. The average group index values are represented by contours.

As the group indices increase, the NDBP values decrease for the chirped PC coupled waveguide structures designed in the directional coupler schemes [30], W1 PCWs with smaller/larger holes in the first rows adjacent to the line-defect [10,11] and W1 PCWs with shifted innermost rows of holes in lateral direction to the waveguide axis [16,17]. However, for fixed s1 values, the NDBP values are observed to be remaining almost the same. When holes are shifted towards the line-defect, a constant NDBP region around 0.3 has been found for group index values between 30 and 90 [18]. In our study, we have found that the NDBP values remain almost constant around 0.28 for the average group index values from 18.6 to 45.2 for s1=-0.02a and s2 between -0.02a and 0.06a. From the contour of n_G values on the NDBP color map, it can be seen that average n_G increases continuously as s1 and s2 increase in positive direction. The maximum

average n_G is found to be 74.42 for (0.02a; 0.08a) configuration. The ring-gap width is calculated as 62 nm for this configuration (for 1.55 μm), which is narrow as is desired for sensing applications [12] and the ring-gaps can be filled with silica by chemical vapor deposition technique or infiltrated with liquid by improved flow-injection systems.

3.2. The group velocity dispersion characteristics

The group velocity dispersion characteristics of the investigated PCWs that show $<n_G>>50$ are illustrated in Fig. 7. If we regard $\beta_2<7.5\text{x}10^3(a/2\pi c^2)$ as ultralow GVD, which is about two orders of magnitude smaller than the estimation given in [31,32], all of the investigated structures show ultralow GVD characteristics. When a is chosen such that 1550 nm wavelength is centered to the minimum of constant n_G-frequency region, the lattice constants change between 379.5 nm and 389.79 nm in the whole scan of s1 and s2 configurations. For the PCW configurations with (-0.02a; 0.08a), (0; 0.08a) and (0.02a; 0.08a), which exhibit highest group index values, the bandwidths corresponding to our ultralow GVD criteria are calculated as 8.21 nm, 5.66 nm and 4.08 nm, respectively by taking into account the values of the corresponding lattice constants. The ultralow GVD criteria value can be much more decreased for the PCW configurations with (0; 0.06a) and (0.02a; 0.06a). If it is reminded that the GVD values are lower for lower group indices, shifting the innermost rows towards the waveguide center appears to be a feasible scheme for relaxing the GVD constraint in slow light PCWs. In addition, the GVD curves exhibit positive and negative β_2 at different normalized frequencies for the same PCW configuration which can be exploited in dispersion compensation applications.

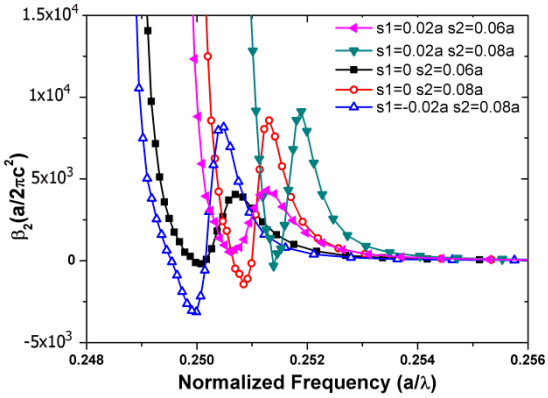

Fig. 7. Group velocity dispersion characteristics of the PCW with one row of ring-shaped holes adjacent to the line - defect for various shifts of first and second innermost rows.

3.3. Temporal pulse shape characteristics

We also investigated the pulse propagation characteristics in time domain for (0.02a; 0.08a) PCW configuration by FDTD simulations [29]. The temporal power profile of H_z fields at input and output detection points is illustrated in Fig. 8. The total length of the PCW is chosen as L=143a and a Gaussian source with a central frequency of 0.251477(2πc/a) is located inside the PCW. The central frequency of the source is adjusted as the minimum point of the constant group index-frequency region and the bandwidth of the source is chosen as the same bandwidth scale of the ±10% n_G range in the PWE calculation. Perfectly-matched layer (PML) absorbing boundary condition is implemented at the limits of the computational domain [33]. The input and output detection points are located at 0.5a and 140.5a, respectively, behind the light source. At the input detection point, the position of the pulse maximum for H_z field in the time axis is noted to be 8112(a/c), while it is 18781(a/c) at the output detection point. The group index is calculated from the total delay between the pulse peaks as 76.21. The group index obtained from the FDTD simulation agrees well with the average group index obtained from PWE calculation. If 1550 is selected as the operating wavelength, the lattice constant should be tuned to 389.79 nm. Using the given lattice constant value, the full-width half-maximum of the pulse is calculated as 4.92 ps at the input detection point and 5.11 ps at the output detection point. This shows that the pulse experiences 3.8% expansion after propagating a distance of 140a (54.57 μm). It is reported that the full-width half-maximum of the pulse broadens 4.17% after propagating a similar propagation distance for a PCW with one row of optimized ring-shaped holes, which supports a group index of 74.4 [14]. This points out that shifting the innermost rows puts forward another degree of optimization in terms of GVD concerns.

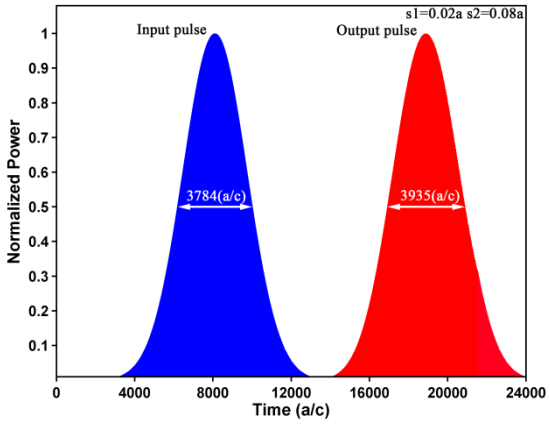

Fig. 8. Time-pulse shapes detected at the input and output detection points for a L=143a PCW with (0.02a; 0.08 a) configuration.

4. Conclusions

A line-defect PCW with one row of ring-shaped holes is designed and the effects of shifting the first two rows towards the line-defect on slow light properties are studied by PWE and FDTD methods. By examining the group

index values, it is found that shifting the second innermost rows together with the first innermost rows is required to reach maximum group index values. In addition, as the second rows shift, the NDBP values remain approximately the same around 0.28 while group index values vary from 18.6 to 45.2. This seems to be an advantage of this approach, if compared to many other slow light approaches in photonic crystal waveguides. When only the first innermost rows are approached to the line-defect, the gap-guided mode of the guided band around $k=0.37(2\pi/a)$ changes its shape from up-facing to down-facing and the group index values increase but this increase is weak. When only the second innermost rows are approached to the line-defect, the major effect occurs in the gap guided mode of guided band and the group index values increase substantially in this case. The shifts of the first and second innermost rows in equal amounts through opposite directions have revealed that the index guided mode of the guided bands follows the shifting behavior of the first innermost rows, while for shifting amounts larger than 0.02a, the gap guided mode of the guided bands follows the shifting behavior of the second innermost rows. In addition, the n_G-frequency curve shape is mainly determined by shifting of first rows, rather than shifting of second rows. Besides, the average group index value of 74.42 obtained from the PWE method is verified using the FDTD method and pulse propagation without apparent waveform distortion is obtained. All these results can open ways to change the shape of the guided band in the desired form for slow light applications of photonic crystals.

Acknowledgements

We gratefully acknowledge the financial support by Scientific Research Projects of Ankara University (BAP) under Grant no. 12B4343011.

References

[1] R. W. Boyd, D. J. Gauthier, A. L. Gaeta, Opt. Photonics News **17**, 18 (2006).
[2] T. F. Krauss, Nat. Photonics, **2**, 448 (2008).
[3] T. Baba, Nat. Photonics, **2**, 465 (2008).
[4] N. Natomi, K. Yamada, A. Shinya, T. Takahashi, C. Takahashi, I. Yokohama, Phys. Rev. Lett. **87**, 253902-1 (2001).
[5] R. J. P. Engelen, Y. Sugimoto, Y. Watanabe, J. P. Korterik, N. Ikeda, N. F. van Hulst, K. Asakawa, L. Kuipers, Opt. Express **14**, 1658 (2006).
[6] A. Y. Petrov, M. Eich, Appl. Phys. Lett. **85**, 4866 (2004).
[7] M. D. Settle, R. J. P. Engelen, M. Salib, A. Michaeli, L. Kuipers, T. F. Krauss, Opt. Express **15**, 219 (2007).
[8] L. H. Frandsen, A. V. Lavrinenko, J. F. Pefersen, P. I. Borel, Opt. Express **14**, 9444 (2006).
[9] F. H. Wang, J. Ma, C. Jiang, J. Lightwave Technol. **26**, 1381 (2008).
[10] S. Kubo, D. Mori, T. Baba, Opt. Lett. **32**, 2981 (2007).
[11] H. Kurt, K. Üstün, L. Ayas, Opt. Express **18**, 26965 (2010).
[12] A. Saynatjoki, M. Mulot, K. Vynck, D. Cassagne, J. Ahopelto, H. Lipsanen, Photonic Nanostruct **6**, 42 (2008).
[13] L. Dai, C. Jiang, J. Lightwave Technol. **27**, 2862 (2009).
[14] J. Hou, D. Gao, H. Wu, R. Hao, Z. Zhou, IEEE Photonic. Tech. L. **21**, 1571 (2009).
[15] Y. Zhai, H. Tian, Y. Ji, J. Lightwave Technol. **29**, 3083 (2011).
[16] R. Hao, E. Cassan, H. Kurt, J. Hou, X. Le Roux, D. Marris-Morini, L. Vivien, D. Gao, Z. Zhou, X. Zhang, IEEE Photonic. Tech. L. **22**, 844 (2010).
[17] R. Hao, E. Cassan, X. L. Roux, D. Gao, V. D. Khanh, L. Vivien, D. Marris-Morrini, Z. Zhang, Opt. Express **18**, 16309 (2010).
[18] J. T. Li, T. P. White, L. O'Faolain, A. Gomez-Iglesias, T. F. Krauss, Opt. Express **16**, 6227 (2008).
[19] J. Wu, Y. P. Li, C. Peng, Z. Y. Wang, Opt. Commun. **283**, 2815 (2010).
[20] J. Liang, L.-Y. Ren, M.-J. Yun, X. Han, X.-J. Wang, J. Appl. Phys. **110**, 063103-1 (2011).
[21] Y. Hamachi, S. Kubo, T. Baba, Opt. Lett. **34**, 1072 (2009).
[22] H. C. Nguyen, S. Hashimoto, M. Shinkawa, T. Baba, Opt. Express **20**, 22465 (2012).
[23] D. M. Beggs, T. P. White, L. Cairns, L. O'Faolain, T. F. Krauss, IEEE Photonic. Tech. L. **21**, 24 (2009).
[24] M. Shinkawa, N. Ishikura,Y. Hama, K. Suzuki, T. Baba, Opt. Express **19**, 22208 (2011).
[25] T. P. White, L. O'Faolain, J. Li, L. C. Andreani, T. F. Krauss, Opt. Express **16**(21), 17076 (2008).
[26] S. A. Schulz, L. O'Faolain, D. M. Beggs, T. P. White, A. Melloni, T. F. Krauss, J. Opt. **12**, 104004-1 (2010).
[27] S. G. Johnson, J. D. Joannopoulos, Opt. Express **8**, 173 (2001).
[28] M. Qui, Appl. Phys. Lett. **81**, 1163 (2002).
[29] A. F. Oskooi, D. Roundy, M. Ibanescu, P. Bermel, J. D. Joannopoulos, S. G. Johnson, Comput. Phys. Commun. **181**, 687 (2010).
[30] D. Mori, S. Kubo, H. Sasaki, T. Baba, Opt. Express **15**, 5264 (2007).
[31] J. Ma, C. Jiang, IEEE Photonic. Tech. L. **20**, 1237 (2008).
[32] D. Wang, J. Zhang, L. Yuan, J. Lei, S. Chen, J. Han, S. Hou, Opt. Commun. **284**, 5829 (2011).
[33] J. P. Berenger, J. Comput. Phys. **114**, 185 (1994).

*Corresponding author: akaoglu@eng.ankara.edu.tr